10. Ubonnut, L. Masters' Thesis, Chulalongkorn University, Bangkok, Thailand, 2005.
11. Starck, P. Polym Int 1996, 40, 111.
12. Allport, D. C.; Janes, W. H., Eds. Block Copolymers; Applied Science Publishers: London; 1973; Chapter 4.
13. Noshay, A.; McGrath, J. E. Block Copolymers, Overview and Critical Survey; Academic Press: New York, 1977: Chapter 5c.
14. Frank, H. P. Polypropylene; Gardon and Breach: New York, 1968.
15. Baldwin, E. P.; Ver Strate, G. Rubber Chem Technol 1972, 45, 709.
16. Jiang, B. Z.; Uhlmann, D. R.; Sande, J. B. V. J Appl Polym Sci 1985, 30, 2485.
17. Yang, D. C.; Zhang, B. L.; Yang, Y. K.; Fang, Z.; Sun, G. F. Polym Eng Sci 1984, 24, 612.
18. Van Gisbergen, J. G. M.; Hoeben, W. F. L. M.; Meijer, H. E. H. Polymer 1991, 31, 1539.
19. Jiang, M. Physical Chemistry in Polymer Alloys; Chengdu, China: Sichuan Educational Press, 1988.
20. McMaster, L. P. Macromolecules 1973, 6, 760.

Korean J. Chem. Eng., 24(3), 397-402 (2007)

Synthesis of nanocrystalline alumina by thermal decomposition of aluminum isopropoxide in 1-butanol and their applications as cobalt catalyst support

Kamonchanok Pansanga, Okorn Mekasuwandumrong*, Joongjai Panpranot and Piyasan Praserthdam†

Center of Excellence on Catalysis and Catalytic Reaction Engineering, Department of Chemical Engineering, Faculty of Engineering, Chulalongkorn University, Bangkok 10330, Thailand
*Department of Chemical Engineering, Faculty of Engineering and Industrial Technology, Silpakorn University, Nakorn Pathom 73000, Thailand
(*Received 21 August 2006 • accepted 13 November 2006*)

Abstract–Nanocrystalline alumina powders were prepared by thermal decomposition of aluminum isopropoxide (AIP) in 1-butanol at 300 °C for 2 h and employed as cobalt catalyst supports. The crystallization of alumina was found to be influenced by the concentration of AIP in the solution. At low AIP content, wrinkled sheets-like structure of γ-Al_2O_3 was formed, while at high AIP concentrations, fine spherical particles of χ-Al_2O_3 were obtained. It was found that using these fine particles alumina as cobalt catalyst supports resulted in much higher amounts of cobalt active sites measured by H_2 chemisorption and higher CO hydrogenation activities.

Key words: Nanocrystalline Alumina, Thermal Decomposition, Cobalt Catalyst, Solvothermal Method, CO Hydrogenation

INTRODUCTION

Alumina powders are very interesting crystalline materials with broad applicability as adsorbents, coatings, soft abrasives, ceramic tools, fillers, wear-resistant ceramics, catalysts, and catalyst supports [1,2]. Because of their fine particle size, high surface area, high melting point (above 2,000 °C), high purity, good adsorbent, and high catalytic activity, they have been employed in a wide range of large-scale technological processes [3,4].

Various transition aluminas (α, γ, χ, δ, η and θ) have been prepared by different methods, such as sol-gel synthesis [5,6], hydrothermal synthesis [7], microwave synthesis [8], emulsion evaporation [9], plasma technique [10], and solvothermal synthesis [11-18]. Among these methods, solvothermal synthesis attracts the most attention because it gives the products with small uniform morphology, well-controlled chemical composition, and narrow size distribution. Furthermore, the desired shape and size of particles can be produced by controlling process conditions such as solute concentration, reaction temperature, reaction time, and the type of solvent [19,20]. For example, Berntsen et al. [21] described a simple route to high surface area nanostructured MoS_2 based on the decomposition of cluster-based precursor $(NH_4)_2Mo_3S_{13}{\cdot}xH_2O$ in toluene at 380 °C. It was found that solvothermal decomposition resulted in nanostructured material distinct from that obtained by decomposition of the precursor in sealed quartz tubes at the same temperature. Wang et al. [22] prepared nanocrystalline titania in alcohols under solvothermal conditions at 100 °C for 24 h. The selection of crystal structures, grain sizes, and morphologies was achieved by simply varying the alcohols and other reaction conditions.

Alumina prepared by the solvothermal method is considered high thermal stability. In our recent works [23-26], nanocrystalline transition alumina with micro spherical particles and high thermal stability has been synthesized by decomposition of aluminum isopropoxide (AIP) under solvothermal conditions. The mechanism of the process involves the formation of amorphous complexes before further decomposition takes place. Inoue et al. [27] prepared silica-modified alumina by the reaction of AIP and tetraethyl orthosilicate (TEOS) in 1,4-butanediol at 300 °C. The products were found to maintain large surface areas after calcination at high temperature.

In this study, the influence of concentration of aluminum isopropoxide in 1-butanol used in the preparation of nanocrystalline alumina by solvothermal method on the properties of alumina powders and alumina supported cobalt catalysts was investigated by using various characterization techniques such as XRD, BET analysis, TEM, SEM, EDX, H_2 chemisorption, and temperature-programmed reduction. The catalytic activity of the catalysts was tested in carbon monoxide hydrogenation at 220 °C and atmospheric pressure.

EXPERIMENTAL

1. Catalyst Preparation

1-1. Preparation of Nanocrystalline Al_2O_3

A selected amount of aluminum isopropoxide (Aldrich) (10-35 g) was suspended in 100 ml of 1-butanol (Ajax Finechem) in a test tube, which was then placed in a 300 ml autoclave. In the gap between the test tube and the autoclave wall, 30 ml of 1-butanol was added. The atmosphere inside the autoclave was purged completely with nitrogen. The mixture was heated to 300 °C at a heating rate of 2.5 °C/min and was kept at that temperature for 2 h. After cooling to room temperature, the resulting powders were collected after repeated washing with acetone by centrifugation. They were then air-dried. The calcination of the products was carried out in a box furnace by heating up to 600 °C at a rate of 10 °C/min and held at that temperature for 1 h.

1-2. Preparation of Al_2O_3-Supported Co Catalysts

The Co/Al_2O_3 catalysts were prepared by incipient wetness impregnation of Al_2O_3 with a desired amount of an aqueous solution

†To whom correspondence should be addressed.
E-mail: piyasan.p@chula.ac.th

of cobalt nitrate [$Co(NO_3)_2 \cdot 6H_2O$] (Aldrich). The final loading of the catalysts was determined by atomic absorption spectroscopy (Varian Spectra A800) to be ca. 10 wt% cobalt. The catalysts were dried at 110 °C for 24 h and calcined in air at 300 °C for 2 h using a ramp rate of 1 °C/min.

2. Catalyst Nomenclature

In this study, alumina and alumina-supported cobalt catalysts are referred to as Al-x and Co/Al-x, where x is the amount (g) of AIP used in the preparation of alumina powders. For example, Al-10 and Co/Al-10 refer to Al_2O_3 and Co/Al_2O_3 catalyst prepared with 10 g AIP.

3. Catalyst Characterization

XRD patterns of the samples were collected with a SIEMENS D-5000 X-ray diffractometer with Cu K_α radiation (λ=1.54439 Å). The spectra were scanned at a rate of 0.04°/step from 2θ=15° to 80°. BET surface areas were calculated by using the BET-single point method at liquid N_2 temperature. Transmission electron microscopy (TEM) was performed with a JEOL JEM1220. SEM and EDX were performed with a JEOL JSM-35CF scanning electron microscope in the back scattering electron (BSE) mode at 20 kV. EDX was performed by using Link Isis 300 software. Static H_2 chemisorption was carried out on the reduced cobalt catalyst samples at 100 °C according to the method described by Reuel and Bartholomew [28] by using a Micromeritics Pulse Chemisorb 2700 system. Prior to H_2 chemisorption, the catalyst samples were reduced at 350 °C in flowing H_2 for 3 h. Temperature-programmed reduction (TPR) was performed by using an in-house system. Approximately 0.1 g of the catalyst was placed in the middle of a stainless steel reactor. A temperature ramp from 35 to 600 °C at a ramp rate 5 °C/min and the reduction gas 5% H_2 in Ar were used. A thermal conductivity detector (TCD) was used to determine the amount of hydrogen consumed. A cold trap was placed before the detector to remove water produced during the reduction. The hydrogen consumption was calibrated by using TPR of silver oxide (Ag_2O) at the same conditions.

4. Reaction

CO hydrogenation was carried out in a fixed-bed quartz reactor under differential reaction conditions (<10% conversion) at 220 °C, 1 atm total pressure, and H_2/CO=10/1. The total flow rate of H_2/CO/Ar was 80/8/32 cc/min. Typically, 0.1 g of the catalyst sample was reduced *in situ* in flowing H_2 (50 cc/min) at 350 °C for 3 h prior to CO hydrogenation. After the startup, samples were taken in 1-h interval and analyzed by gas chromatography. Steady state was reached within 6 h in all cases.

RESULTS AND DISCUSSION

1. Effect of AIP Concentration on the Properties of Al_2O_3

Fig. 1 shows the XRD patterns of various alumina powders obtained from thermal decomposition of AIP in 1-butanol after calcination at 600 °C for 1 h. XRD patterns of Al_2O_3 show strong diffraction peaks at 31°, 33°, 38°, 43°, 47.5°, and 68° (according to the JCPDSs database). It was found that when lower amounts of AIP were used, only γ-alumina was formed as seen by the XRD characteristic peaks at 2θ=33° according to the JCPDSs database. The XRD characteristic peaks of χ-alumina were observed at 2θ=42.5° for the ones prepared with AIP 25 and 35 g. The intensity of χ-alumina peaks became stronger with increasing amount of AIP content. It is indicated that increasing AIP content during the synthesis resulted in formation of mixed phase between γ-alumina and χ-alumina. The crystallization process of alumina was probably affected by the amounts of AIP in 1-butanol.

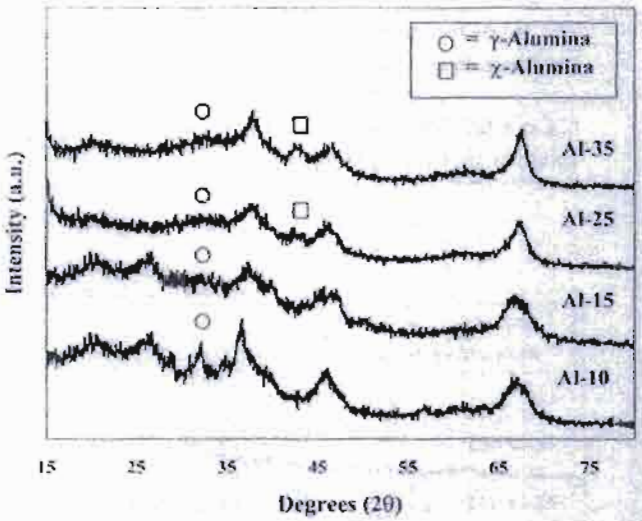

Fig. 1. XRD patterns of various nanocrystalline alumina prepared by the reaction of AIP in 1-butanol at 300 °C for 2 h (after calcinations at 600 °C for 1 h).

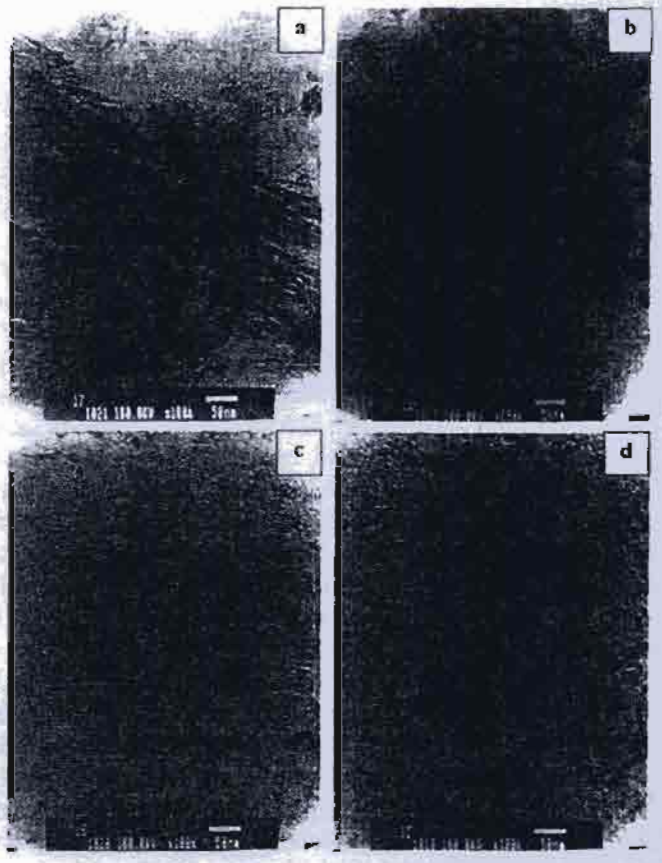

Fig. 2. TEM images of alumina obtained by the reaction of AIP in 1-butanol at 300 °C for 2 h with different amounts of AIP (a) Al-10 (b) Al-15 (c) Al-25 (d) Al-35.

Table 1. The physical and chemical properties of Al_2O_3 supports

Samples	Amounts of AIP (g)	Surface area (m^2/g)*	Bulk density (g/cm^3)*	Morphology
Al-10	10	70	0.3824	Wrinkled sheets
Al-15	15	120	0.3858	High amount of wrinkled sheets
Al-25	25	139	0.3928	Wrinkled sheets and small amount of spherical particles
Al-35	35	145	0.5358	Small amount of wrinkled sheets and high amount of spherical particles

*Error of measurement=±5%

TEM images of alumina powders prepared with different amounts of AIP are shown in Fig. 2. For the ones prepared with lower amounts of AIP, Al-10 and Al-15, the wrinkled sheets morphology was observed. They were found to be similar to those obtained from the formation of γ-alumina by decomposition of glycol or alkyl derivatives on boehmite [26,27]. As the amounts of AIP increased, the wrinkled sheets morphology became less apparent and spherical particles were observed. The presence of spherical particles was probably due to the formation of χ-alumina, which is normally formed by thermal decomposition reaction of AIP in inert organic solvents at 300 °C [23-26]. TEM results were in good agreement with the XRD patterns that a mixture of γ-alumina and χ-alumina was observed when AIP concentration increased.

The physical properties of the alumina products are summarized in Table 1. The BET surface areas increased with increasing AIP concentration as a result of morphology changing from wrinkled sheets structure to small spherical particles. BET surface area of the Al-35 (145 m^2/g) was found to be twice of that of Al-10 (70 m^2/g). Similar trend was observed for the bulk density of the alumina powders. The bulk density increased with increasing AIP contents.

Mechanism of thermal decomposition of AIP in alcohol has been proposed in our previous works [23,26] involving three competitive reactions. First, AIP reacted with 1-butanol yielding aluminum butoxide, which decomposed further to give the alkyl (butyl) derivative of boehmite. Second, 1-butanol can be dehydrated to give water which then hydrolyzes aluminum isopropoxide or butoxide yielding pseudoboehmite. Finally, the direct decomposition of aluminum alkoxide in organic solvent, which proceeded slowest, gave χ-alumina. In the present work, at low AIP content, boehmite was probably the main product and γ-alumina was obtained after calcination at 600 °C for 1 h. The morphology of the boehmite products obtained via solvothermal reaction was wrinkled sheets [23,26], which was also similar to those of γ-alumina decomposed from. However, when the amounts of AIP in 1-butanol increased, formation of χ-alumina from direct decomposition of AIP in the solvent occurred as the main reaction.

2. Characteristics of Co/Al_2O_3 Catalysts

The XRD patterns of cobalt catalysts supported on alumina prepared with various amounts of AIP are shown in Fig. 3. The XRD patterns of the Co/Al_2O_3 catalysts were not significantly different from those of alumina supports. No XRD peaks of Co_3O_4 or other Co compounds were detected. This indicates that cobalt was present in a highly dispersed form on alumina even for cobalt loading as high as 10 wt% [29].

SEM and EDX were performed in order to study the morphology and elemental distribution of the catalyst samples, respectively. Typical SEM micrographs of Co/Al_2O_3 catalysts are shown in Fig. 4. There was no significant change in morphology of the catalyst samples due to the effect of AIP concentrations in 1-butanol used in the preparation process. The white or light spots observed in all figures can be attributed to the cobalt patches distributed on the external surface of catalyst granules. Fig. 5 shows the SEM micrographs and the EDX mapping of the cross-sectioned Co/Al-35 catalyst granule. The distribution of cobalt was found to be well dispersed throughout the catalyst granule.

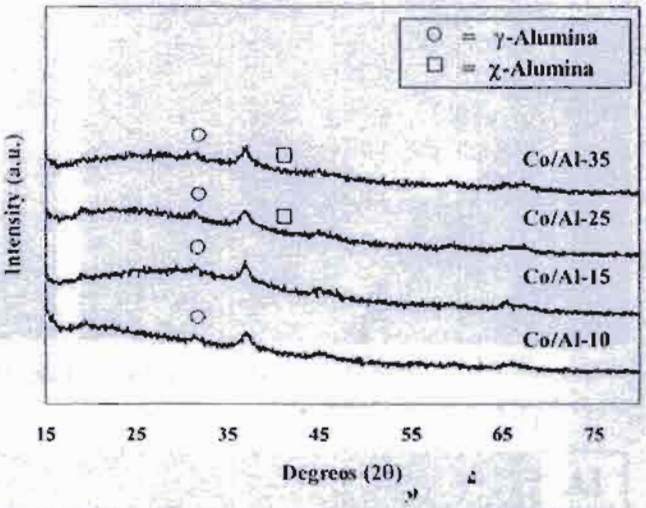

Fig. 3. XRD patterns of Co/Al_2O_3 catalysts with different amounts of AIP.

The relative amounts of active surface cobalt on the catalyst samples were calculated from H_2 chemisorption experiments at 100 °C according to Reuel and Bartholomew [28]. It is known that only surface cobalt metal atoms are active for CO hydrogenation, not its oxide or carbide [30]. The H_2 chemisorption results are reported in Table 2. The amounts of H_2 chemisorption increased from 0.90 to 20.65 μmol/g cat., with increasing amount of AIP in 1-butanol used in the preparation of the alumina supports from 10 to 35 g. It is likely that the increase in the relative amounts of active cobalt metals was due to the formation of the small spherical particles of χ-alumina. As also seen in the Table 2, the amount of H_2 chemisorption of Co/Com-Al (13.38 μmol/g cat.), prepared from the commercial γ-alumina which the crystal shape of alumina was spherical (the results was not shown), was better than solvothermal-made Co/γ-alumina (0.90 μmol/g cat.) but lower than Co/χ-alumina (20.65 μmol/g cat.).

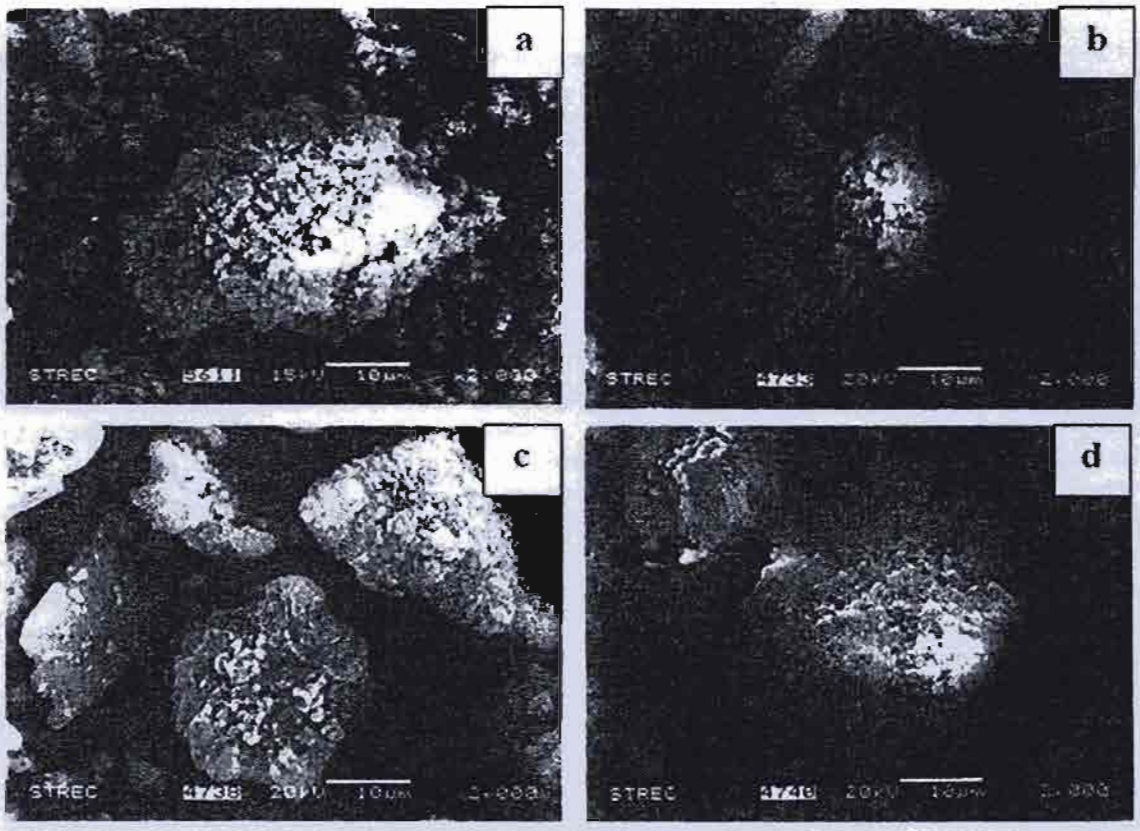

Fig. 4. SEM micrographs of (a) Co/Al-10, (b) Co/Al-15, (c) Co/Al-25, and (d) Co/Al-35.

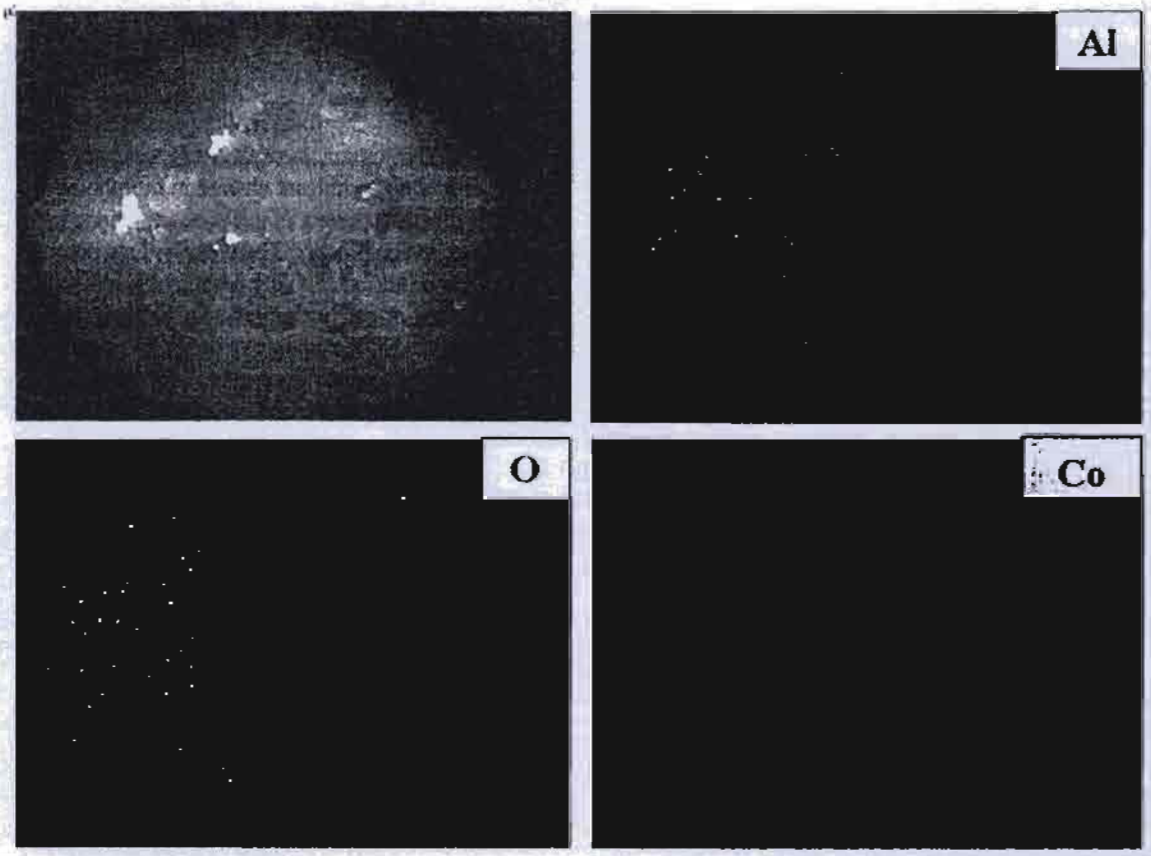

Fig. 5. SEM micrograph and EDX mapping of cross-sectioned Co/Al-35 catalyst granule.

It was again confirmed that the spherical morphology of the alumina support is important in achieving a higher amount of active cobalt metal.

3. Reduction and Catalytic Behaviors of Co/Al_2O_3 Catalysts

Temperature program reduction (TPR) is a powerful tool for studying the reduction behavior of the catalysts. The TPR profiles of various nanocrystalline alumina supported cobalt catalysts are shown in Fig. 6. All the catalyst samples exhibited two main reduction peaks which could be assigned to the two-step reduction of Co_3O_4: first reduction of Co_3O_4 to CoO and then the subsequent reduction of CoO to Co^0 [31]. The two reduction steps may not always be observed as separate peaks in TPR profile [32], as seen in the Co/Al-35 sample. A wide range of variables such as metal particle size and metal-support interaction have an influence on the reduction behavior of cobalt catalysts resulting in the observation of different locations of the TPR peaks. The TPR profiles for all the catalysts except Co/Al-35 appeared to be not significantly different, suggesting that the AIP content had little impact on the interaction of cobalt and alumina supports. Thus, high dispersion of cobalt obtained on Co/Al-35 was rather to be due to the formation of small spherical particles alumina and not to the change in reducibility of the catalysts.

Table 2. The characteristics and H_2 chemisorption of cobalt catalyst

Catalyst samples	Surface area (m^2/g)[a]	Amount of H_2 chemisorption ($\mu mol/g$ cat.)[a]
Co/Al-10	61	0.90
Co/Al-15	87	2.29
Co/Al-25	108	7.58
Co/Al-35	114	20.65
Co/Com-Al*	145	13.38

[a]Error=±5%, as determined directly.
*Commercial γ-alumina, BET surface area of alumina 230 m^2/g.

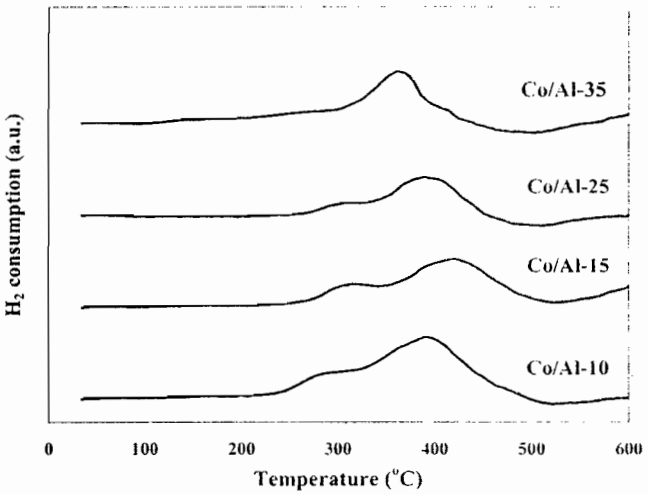

Fig. 6. TPR profiles of the catalyst samples.

CO hydrogenation reaction was carried out as a test reaction to determine the catalytic activity of the catalyst samples. The results are shown in Table 3. It is clearly seen that alumina prepared with higher amounts of AIP in 1-butanol resulted in much higher CO hydrogenation activities and CH_4 selectivities. The reaction results confirm the amount of surface cobalt metals measured by H_2 chemisorption.

CONCLUSIONS

Nanocrystalline alumina powders were prepared by thermal decomposition of AIP in 1-butanol with various AIP contents. The concentration of AIP in 1-butanol had a significant impact on the properties of alumina and alumina supported cobalt catalysts. Increasing amounts of AIP in the solution resulted in the transformation of wrinkled sheet γ-alumina to fine spherical particles of χ-alumina. It also gave rise to the cobalt active sites and CO hydrogenation activities when employed as supports for preparation of Co/Al_2O_3 catalysts.

ACKNOWLEDGMENTS

The authors would like to thank the Thailand Research Fund (TRF) for the financial support of this project.

REFERENCES

1. J. S. Church, N. W. Cant and D. L. Trimm, *Appl. Catal. A*, **101**(1), 105 (1993).
2. G. Pajonk and S. Teichner, *Aerogels*, Spinger, Berlin (1986).
3. C. Misra, *Industrial alumina chemicals*, ACS Monograph 184, Washington (1986).

Table 3. Reaction rate and selectivity for CO hydrogenation on catalyst samples

Catalyst samples	CO conversion (%)[a]		Rate ($\times 10^2$ gCH_2 $gcat^{-1}h^{-1}$)[b]		CH_4 selectivity (%)	
	Initial[c]	SS[d]	Initial	SS	Initial	SS
Co/Al-10	1.92	0.54	5.76	1.62	13	11
Co/Al-15	2.63	0.75	7.89	2.25	49	47
Co/Al-25	5.45	3.02	16.35	9.06	56	54
Co/Al-35	8.49	4.03	25.47	12.09	70	67

[a]CO hydrogenation was carried out at 220 °C, 1 atm, and H_2/CO/Ar=80/8/32.
[b]Error±5%, as determined directly.
[c]After 20 min of reaction.
[d]After 6 h of reaction.

4. H. Topsoe, B. S. Clausen and F. E. Massoth, *Hydrotreating catalysis*, Springer, Berlin (1996).
5. C. J. Brinker and G. W. Scherrer, *Sol-gel science*, Academic Press, San Diego (1990).
6. K.-C. Song, K.-J. Woo and Y. Kang, *Korean J. Chem. Eng.*, **16**, 75 (1999).
7. W. H. Dawson, *Am. Ceram. Soc. Bull.*, **67**, 1673 (1988).
8 S. G. Deng and Y. S. Lin, *Sci. Lett.*, **16**, 1291 (1997).
9. Y. Sarikaya, I. Sevinc and M. Akinc, *Powder Technol.*, **116**(1), 109 (2001).
10. S.-M. Oh and D.-W. Park, *Korean J. Chem. Eng.*, **17**, 299 (2000).
11. M. Inoue, H. Kominami and T. Inui, *J. Am. Ceram. Soc.*, **73**, 1100 (1990).
12. M. Inoue, H. Kominami and T. Inui, *J. Chem. Soc. Dalton Trans.*, 3331 (1991).
13. M. Inoue, H. Kominami and T. Inui, T. *J. Am. Ceram. Soc.*, **75**, 2597 (1992).
14. M. Inoue, H. Kominami and T. Inui, *Appl. Catal. A*, **97**, L25 (1993).
15. M. Inoue, H. Kominami and T. Inui, *Appl. Catal. A*, **121**, L1 (1995).
16. M. Inoue, H. Kominami and T. Inui, *J. Am. Ceram. Soc.*, **75**, 2597 (1996a).
17. M. Inoue, Y. Kondo and T. Inui, *Inorg. Chem.*, **27**, 215 (1988).
18. M. Inoue, H. Otsu, H. Kominami and T. Inui, *Ind. Eng. Chem. Res.*, **35**, 295 (1996b).
19. Y. Deng, G-D. Wei and C.-W. Nan, *Chem. Phys. Lett.*, **368**(5-6), 639 (2003).
20. Y. Deng, X.-S. Zhou, G-D. Wei, J. Liu, C.-W. Nan and S.-J. Zhao, *J. Phys. Chem. Solids*, **63**(11), 2119 (2002).
21. N. Berntsen, T. Gutjahr, L. Loeffler, J. R. Gomm, R. Seshadri and W. Tremel, *Chem. Mater.*, **15**(23), 4498 (2003).
22. C. Wang, Z.-X. Deng, G. Zhang, S. Fan and Y. Li, *Powder Technol.*, **125**(1), 39 (2002.
23. O. Mekasuwandumrong, H. Kominami, P. Praserthdam and M. Inoue, *J. Am. Ceram. Soc.*, **87**(8), 1543 (2004a).
24. O. Mekasuwandumrong, P. Praserthdam, M. Inoue, V. Pavarajarn and W. Tanakulrungsank, *J. Mater. Sci.*, **39**, 2417 (2004b).
25. O. Mekasuwandumrong, P. L. Silveston, P. Praserthdam, M. Inoue, V. Pavarajarn and W. Tanakulrungsank, *Inorg. Chem. Commu.*, **6**(7), 930 (2003).
26. P. Praserthdam, M. Inoue, O. Mekasuvandumrong, W. Tanakulrungsank and S. Phatanasri, *Inorg. Chem. Commu.*, **3**(11), 671 (2000).
27. M. Inoue, H. Otsu, H. Kominami and T. Inui, *Ind. Eng. Chem. Res.*, **35**, 295 (1996c).
28. R. C. Reuel and C. H. Bartholomew, *J. Catal.*, **85**, 63 (1984).
29. B. Jongsomjit, J. Panpranot and J. G. Goodwin Jr., *J. Catal.*, **215**(1), 66 (2003).
30. R. B. Anderson, *The Fischer-Tropsch synthesis*, Academic Press, San Diego (1984).
31. Y. Zhang, D. Wei, S. Hammache and J. G. Goodwin Jr., *J. Catal.*, **188**(2), 281 (1999).
32. B. Ernst, S. Libs, P. Chaumette and A. Kiennemann, *Appl. Catal. A*, **186**(1-2), 145 (1999).

4. H. Topsoe, B. S. Clausen and F. E. Massoth, *Hydrotreating catalysis*, Springer, Berlin (1996).
5. C. J. Brinker and G. W. Scherrer, *Sol-gel science*, Academic Press, San Diego (1990).
6. K.-C. Song, K.-J. Woo and Y. Kang, *Korean J. Chem. Eng.*, **16**, 75 (1999).
7. W. H. Dawson, *Am. Ceram. Soc. Bull.*, **67**, 1673 (1988).
8 S. G. Deng and Y. S. Lin, *Sci. Lett.*, **16**, 1291 (1997).
9. Y. Sarikaya, I. Sevinc and M. Akinc, *Powder Technol.*, **116**(1), 109 (2001).
10. S.-M. Oh and D.-W. Park, *Korean J. Chem. Eng.*, **17**, 299 (2000).
11. M. Inoue, H. Kominami and T. Inui, *J. Am. Ceram. Soc.*, **73**, 1100 (1990).
12. M. Inoue, H. Kominami and T. Inui, *J. Chem. Soc. Dalton Trans.*, 3331 (1991).
13. M. Inoue, H. Kominami and T. Inui, T. *J. Am. Ceram. Soc.*, **75**, 2597 (1992).
14. M. Inoue, H. Kominami and T. Inui, *Appl. Catal. A*, **97**, L25 (1993).
15. M. Inoue, H. Kominami and T. Inui, *Appl. Catal. A*, **121**, L1 (1995).
16. M. Inoue, H. Kominami and T. Inui, *J. Am. Ceram. Soc.*, **75**, 2597 (1996a).
17. M. Inoue, Y. Kondo and T. Inui, *Inorg. Chem.*, **27**, 215 (1988).
18. M. Inoue, H. Otsu, H. Kominami and T. Inui, *Ind. Eng. Chem. Res.*, **35**, 295 (1996b).
19. Y. Deng, G-D. Wei and C.-W. Nan, *Chem. Phys. Lett.*, **368**(5-6), 639 (2003).
20. Y. Deng, X.-S. Zhou, G-D. Wei, J. Liu, C.-W. Nan and S.-J. Zhao, *J. Phys. Chem. Solids*, **63**(11), 2119 (2002).
21. N. Berntsen, T. Gutjahr, L. Loeffler, J. R. Gomm, R. Seshadri and W. Tremel, *Chem. Mater.*, **15**(23), 4498 (2003).
22. C. Wang, Z.-X. Deng, G. Zhang, S. Fan and Y. Li, *Powder Technol.*, **125**(1), 39 (2002.
23. O. Mekasuwandumrong, H. Kominami, P. Praserthdam and M. Inoue, *J. Am. Ceram. Soc.*, **87**(8), 1543 (2004a).
24. O. Mekasuwandumrong, P. Praserthdam, M. Inoue, V. Pavarajarn and W. Tanakulrungsank, *J. Mater. Sci.*, **39**, 2417 (2004b).
25. O. Mekasuwandumrong, P. L. Silveston, P. Praserthdam, M. Inoue, V. Pavarajarn and W. Tanakulrungsank, *Inorg. Chem. Commu.*, **6**(7), 930 (2003).
26. P. Praserthdam, M. Inoue, O. Mekasuvandumrong, W. Tanakulrungsank and S. Phatanasri, *Inorg. Chem. Commu.*, **3**(11), 671 (2000).
27. M. Inoue, H. Otsu, H. Kominami and T. Inui, *Ind. Eng. Chem. Res.*, **35**, 295 (1996c).
28. R. C. Reuel and C. H. Bartholomew, *J. Catal.*, **85**, 63 (1984).
29. B. Jongsomjit, J. Panpranot and J. G. Goodwin Jr., *J. Catal.*, **215**(1), 66 (2003).
30. R. B. Anderson, *The Fischer-Tropsch synthesis*, Academic Press, San Diego (1984).
31. Y. Zhang, D. Wei, S. Hammache and J. G. Goodwin Jr., *J. Catal.*, **188**(2), 281 (1999).
32. B. Ernst, S. Libs, P. Chaumette and A. Kiennemann, *Appl. Catal. A*, **186**(1-2), 145 (1999).

Available online at www.sciencedirect.com
ScienceDirect
Materials Letters 61 (2007) 1376–1379
materials letters
www.elsevier.com/locate/matlet

Effect of nanoscale SiO_2 and ZrO_2 as the fillers on the microstructure of LLDPE nanocomposites synthesized via *in situ* polymerization with zirconocene

Bunjerd Jongsomjit *, Joongjai Panpranot, Piyasan Praserthdam

Center of Excellence on Catalysis and Catalytic Reaction Engineering, Department of Chemical Engineering, Faculty of Engineering, Chulalongkorn University, Bangkok 10330, Thailand

Received 7 February 2006; accepted 13 July 2006
Available online 1 August 2006

Abstract

In the present study, the nanoSiO_2 and nanoZrO_2 were used as the fillers for linear low-density polyethylene (LLDPE) nanocomposites. In fact, the LLDPE nanocomposites were synthesized via the *in situ* polymerization of ethylene/1-octene with a zirconocene/MAO catalyst in the presence of the fillers. The LLDPE–nanocomposites were further characterized by means of TEM, DSC, ^{13}C NMR and XPS. It was found that productivity increased more when the nanoZrO_2 filler was applied. The similar distribution for both fillers was observed by TEM. Based on the ^{13}C NMR results, it appeared that the LLDPE nanocomposites obtained from both fillers were random copolymer. In particular, the resulted binding energy and elemental concentration at surface obtained from XPS measurement were further discussed in more details.

Keywords: Polymer nanocomposite; Nanofillers; Metallocene; LLDPE; XPS

1. Introduction

Polymer composites are important commercial materials with various applications. It is known that materials or fillers with synergistic properties can be selected to create the polymer composites with desired properties. However, upon the significant development of nanoscience and nanotechnology in the recent years, nanoscale fillers have brought attraction to research in polymer composite. As known, polymers filled with nanoscale fillers are recognized as polymer nanocomposites. Apparently, with addition of nanoscale fillers into polymers, robust materials can potentially be produced due to the synergistic effects (cooperating for enhanced effects) arising from the blending process. In general, there are technically three methods used to produce a polymer composite; (i) a melt mixing [1–5], (ii) a solution blending [6] and (iii) *in situ* polymerization [7]. Due to the direct synthesis via polymerization along with the presence of fillers, the *in situ* polymerization is perhaps considered the most promising technique to produce polymer nanocomposites with homogeneous dispersion of nanoscale fillers inside the polymer matrix. Based on the commercial interest of using metallocene catalysts for olefin polymerization, it has led to an extensive effort for utilizing metallocene catalysts efficiently [8–11]. With a combination of knowledge in nanotechnology, polymerization, and metallocene catalysis, a promising way to synthesize the polymer nanocomposites using a metallocene catalyst is captivating.

In our previous work [12], we revealed that LLDPE nanocomposites could be synthesized via the *in situ* polymerization with a zirconocene/MAO catalyst. However, our present study focussed on further development in order to give a better understanding on how different nanoscale fillers could interact inside the polymer matrix. Obviously, this can result in different properties of polymer nanocomposites obtained.

2. Experimental

All chemicals [ethylene (99.96%) donated by the National Petrochemical of Thailand, toluene (Exxon), *rac*-ethylenebis (indenyl) zirconium dichloride [*rac*-Et$(Ind)_2ZrCl_2$] from Aldrich, methylaluminoxane (MAO, 2.67 M in toluene) donated by the

* Corresponding author. Tel.: +66 2 2186869; fax: +66 2 2186877.
E-mail address: bunjerd.j@chula.ac.th (B. Jongsomjit).

0167-577X/$ - see front matter © 2006 Elsevier B.V. All rights reserved.
doi:10.1016/j.matlet.2006.07.034

Table 1
Characteristics of LLDPE nanocomposites

Characteristics	LLDPE–$nanoSiO_2$	LLDPE–$nanoZrO_2$
1) Productivity (kg polymer/mol cat. h)	1319	6924
2) Melting temperature, T_m (°C)	90	94
3) Copolymer type (obtained from ^{13}C NMR)	Random	Random
4) C 1s binding energy (eV)	286.5	285.7

Tosoh Akso, Japan, trimethylaluminum (TMA, 2.0 M in toluene) from Nippon Alkyls, Japan, 1-octene (98%, Aldrich), $nanoSiO_2$ (Aldrich) and $nanoZrO_2$ fillers] were manipulated under an inert atmosphere using a vacuum glove box and/or the Schlenk techniques. 1-Octene was purified by distilling over sodium under argon atmosphere. Toluene was dried over dehydrated $CaCl_2$ and distilled over sodium benzophenone under argon atmosphere prior to use.

The $nanoZrO_2$ filler was synthesized by flame spray pyrolysis (FSP) as described by Mueller et al. [13]. The primary particle size of ZrO_2 was in the range of 6–35 nm. The crystal structure consisted of the tetragonal/monoclinic phase (95/5 by mol%). The $nanoSiO_2$ filler was obtained from Aldrich (30–40 nm). First, 1 g of the filler reacted with a desired amount of MAO in toluene at room temperature and was stirred for 30 min. The solvent was then removed from the mixture. About 20 ml of toluene was added into the obtained precipitate, the mixture was stirred for 5 min, and then the solvent was removed. This procedure was done for 5 times to ensure the removal of impurities. The white powder of nanoscale filler-impregnated MAO was obtained.

The ethylene/1-octene copolymerization reaction on the filler-impregnated MAO was carried out in a 100-ml semi-batch stainless steel autoclave reactor equipped with a magnetic stirrer. At first, 0.3 g of the nanoscale filler-impregnated MAO ($[Al]_{MAO}/[Zr]=3405$) and 0.018 mol of 1-octene along with toluene (to make a total volume of 30 ml) were put into the reactor. The desired amount of *rac*-$Et(Ind)_2ZrCl_2$ (5×10^{-5} M) and TMA ($[Al]_{TMA}/[Zr]=2500$) was mixed and stirred for 5 min aging at room temperature, separately, then was injected into the reactor. The reactor was heated up to polymerization temperature at 70 °C. To start reaction, 0.018 mol of ethylene was fed into the reactor. After, all ethylene was consumed, the reaction was terminated by addition of acidic methanol. After filtration, washing with methanol and drying at room temperature, white powder of $nanoZrO_2$ (SiO_2)-filled polymer was obtained.

The polymer sample was then characterized using the differential scanning calorimetry; DSC (NETZSCH DSC 200), transmission electron microscopy; TEM (JEOL-TEM 200CX), X-ray photoelectron spectroscopy; XPS (Shimadzu AMICUS with VISION 2 control software), and ^{13}carbon nuclear magnetic resonance; ^{13}C NMR (JEOL JMR-A500).

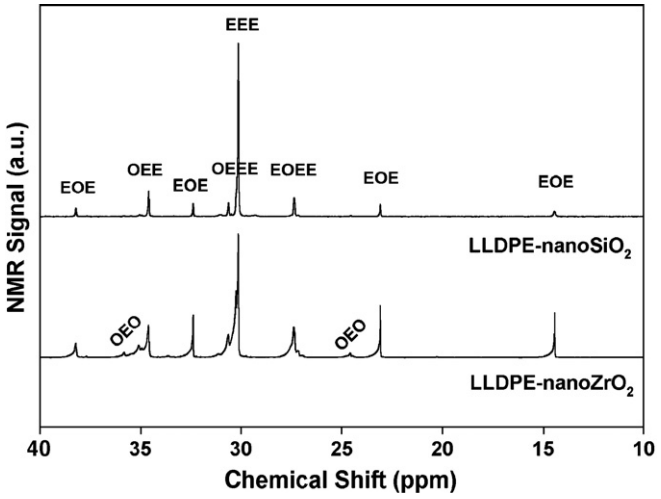

Fig. 2. ^{13}C NMR spectra of the LLDPE–$nanoSiO_2$ and LLDPE–$nanoZrO_2$ and their triad distribution identification (**E** refers to the ethylene sequence and **O** refers to the 1-octene sequence).

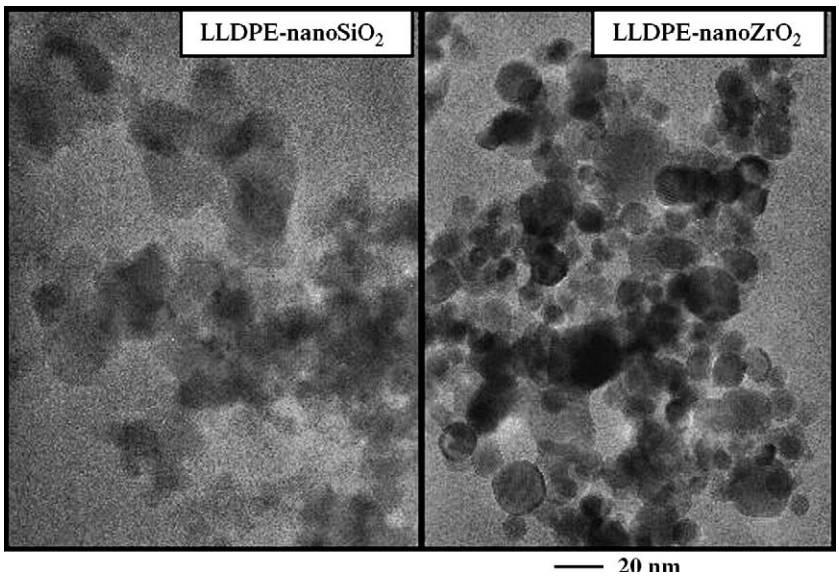

Fig. 1. TEM micrographs of the LLDPE–$nanoSiO_2$ and LLDPE–$nanoZrO_2$.

3. Results and discussion

In the present study, we synthesized the LLDPE–nanoSiO_2 and LLDPE–nanoZrO_2 composites via the *in situ* polymerization with a zirconocene/MAO catalyst. At low amounts of the MAO impregnated-fillers, the activities of catalyst were very low. Hence, the amount of filler at 0.3 g which was corresponding to the ratio of $[Al]_{MAO}/[Zr]=3405$ was applied. After polymerization, the white powder of LLDPE nanocomposites was obtained. The characteristics of LLDPE nanocomposites are shown in Table 1. It was found that the productivity of LLDPE–nanoZrO_2 synthesized via this specified condition was much higher than that of the LLDPE–nanoSiO_2 about 5 times. This was probably due to the strong interaction between MAO and the nano-SiO_2. The melting temperature (T_m) obtained by DSC showed only slight difference in T_m of the two samples. As known, images from high resolution transmission electron microscopy (TEM) are an essential component of nanoscience and nanotechnology, therefore, TEM was performed in order to determine the distribution and dispersion of fillers. The TEM images of the LLDPE–SiO_2 and LLDPE–ZrO_2 are shown in Fig. 1. As seen from both two images, the nanoscale fillers appeared as a group of spherical-like particles indicating the agglomeration of the primary particles. It only indicated that the nanoscale fillers were well distributed inside the polymer matrix, but somehow were poorly dispersed due to the agglomeration. There was no significant difference based on the TEM images for the LLDPE–nanoSiO_2 and LLDPE–nanoZrO_2.

Among a number of important aspects for making a polymer composite, one has to mention how the microstructure of polymer is altered with the addition of nanoscale fillers. Technically, the nanoscale fillers added should not affect the polymer microstructure, but only change the physical properties based on the macroscopic point of view. It has been known that up to now ^{13}C NMR is one of the most powerful techniques used to identify the microstructure of polymer, especially polyolefins. The ^{13}C NMR spectra obtained from LLDPE–nanoSiO_2 and LLDPE–nanoZrO_2 are shown in Fig. 2. The resulted ^{13}C NMR spectra were assigned typically to the LLDPE obtained from the copolymerization of ethylene/1-octene. The triad distribution was identified based on the method reported by Randall [14] where **E** refers to the ethylene sequence and **O** refers to the 1-octene sequence. It can be observed that both samples exhibited the similar ^{13}C NMR patterns indicating the similar molecular structure. Upon the calculation described by Galland et al. [15], the distribution of comonomer was random as also shown in Table 1. This was similar to what we have found in our previous work when no filler was added [10]. However, as seen from Fig. 2, it showed that the degree of 1-octene incorporation for LLDPE–nanoZrO_2 was slightly higher.

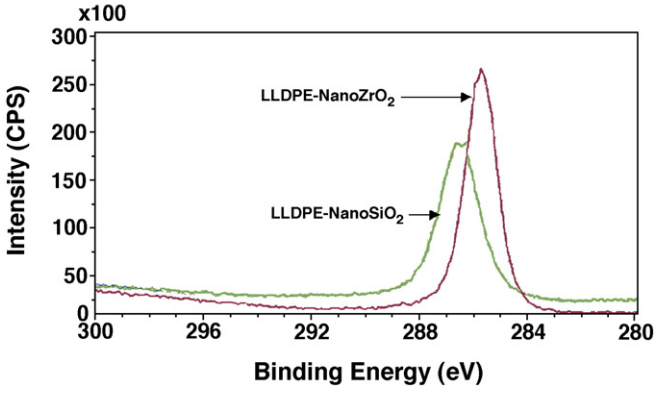

Fig. 3. A plot of binding energy for C 1s obtained from XPS of LLDPE–nanoSiO_2 and LLDPE–nanoZrO_2.

Table 2
Elemental distribution on the surface of LLDPE nanocomposite and the binding energy measured by XPS

Polymer nanocomposite	Peak	B.E. (eV)	FWHM (eV)	Atomic conc. (%)	Mass conc. (%)
LLDPE–nanoZrO_2	O 1s	533.3	1.386	1.79	2.37
	C 1s	285.7	1.419	98.19	97.47
	Zr 3d	185.7	0.756	0.02	0.16
LLDPE–nanoSiO_2	O 1s	534.3	2.368	29.99	32.35
	C 1s	286.5	1.740	59.90	48.50
	Si 2p	104.6	1.944	10.11	19.15

Although ^{13}C NMR showed that the molecular structure of polymer did not change upon the addition of the nanoscale fillers, it cannot differentiate interaction arising from different fillers inside the polymer matrix. Hence, a more powerful characterization technique was necessary for such a purpose. Here, we used the X-ray photoelectron spectroscopy (XPS) to identify different interactions inside the polymer matrix. Since XPS is one of the most powerful techniques used for many applications in surface analysis, so it is also interesting to extend the use of XPS in order to probe the different interactions of the polymer nanocomposites. A plot of the binding energy (BE) for C 1s obtained from XPS for both LLDPE–nanoSiO_2 and LLDPE–nano-ZrO_2 is shown in Fig. 3. BE for the LLDPE–nanoSiO_2 was found to be 286.5 eV whereas the BE for LLDPE–nanoZrO_2 was 285.7 eV (Table 1). Obviously, as seen from Fig. 3, the shift of BE was observed with different nanoscale fillers due to perhaps a different interaction between the fillers and polymer matrix. In fact, the binding energy between 285.7 and 286.5 eV was assigned to the C–C bond in the polymer chain under a different environment. It must be noted that the samples used in this study are insulators. The insulators are always a problem in XPS due to the sample charging. The problem can be partially alleviated, but shifts in BE of several eV can still occur in the presence of charging. To overcome the charging problem, the samples must be coated with a very thin layer of gold by sputtering. It is common practice in XPS to refer the BE to the C 1s electrons that are to be measured. Hence, the energy reference for Ag metal (368.0 eV for $3d_{5/2}$) was used in this study. Besides the BE obtained from XPS, the amounts of Si and Zr atomic and mass concentrations at surface (the depth for XPS is ca. 5 nm) were also determined as shown in Table 2. Surprisingly, with the same amount (0.3 g) of the nanoscale fillers added to the polymer, the penetration of them was totally different. As seen in Table 2 for the mass concentrations, it can be observed that only 0.16% of Zr was found at the surface. This indicated that the ZrO_2 filler penetrated more deeply into the polymer matrix. In contrast, it was found that 19.15% of Si was present at the surface. It was suggested that the SiO_2 filler preferred to be located on the surface more. Therefore, a different location of fillers in the polymer matrix would result in a different interaction indicating the slight shift of BE of the C–C bond in the polymer chain as seen by XPS.

4. Summary

In summary, the LLDPE–nanoSiO_2 and LLDPE–nanoZrO_2 were synthesized via *in situ* polymerization using a zirconocene/MAO catalyst. With the use of nanoZrO_2, the productivity increased more pronouncedly about 5 times. The distribution of both nanoscale fillers obtained from TEM was similar. It also

showed that both LLDPE–nanocomposites exhibited the similar ^{13}C NMR spectra indicating that only random copolymer was obtained. In particular, the XPS measurement indicated only a slightly different interaction for those LLDPE–nanocomposites. It was found that the different location of the nanoscale fillers rendered the BE shift of the C–C bond in the polymer chain.

Acknowledgments

We thank the National Science and Technology Development Agency (NSTDA), the Thailand–Japan Technology Transfer Project (TJTTP-OECF), and the Thailand Research Fund (TRF) for the financial support of this project. We also thank Dr. Okorn Mekasuwandumrong for providing the nanoZrO_2 filler used in this study.

References

[1] C.J.R. Verbeek, Mater. Lett. 56 (2002) 226–231.
[2] R. Nawang, I.D. Danjaji, U.S. Ishiaku, H. Ismail, Z.A.M. Ishak, Polym. Test. 20 (2001) 167–172.
[3] Y. Haung, Y.Q. Zhang, Y.Q. Hua, J. Mater. Sci. Lett. 22 (2003) 997–998.
[4] I.D. Danjaji, R. Nawang, U.S. Ishiaku, H. Ismail, Z.A.M. Ishak, Polym. Test. 21 (2002) 75–81.
[5] C.J.R. Verbeek, Mater. Lett. 52 (2002) 453–457.
[6] G.B. Rossi, G. Beaucage, T.D. Dang, R.A. Vaia, Nano Lett. 2 (4) (2002) 319–323.
[7] T.K. Mandal, M.S. Fleming, D.R. Walt, Nano Lett. 2 (1) (2002) 3–7.
[8] C.L.P. Shan, J.B.P. Soares, A. Penlidis, Polym. Chem. 40 (2002) 4426–4451.
[9] K.L. Chu, C.L.P. Shan, J.B.P. Soares, A. Penlidis, Macromol. Chem. Phys. 200 (1999) 2372–2376.
[10] B. Jongsomjit, P. Kaewkrajang, P. Praserthdham, Mater. Chem. Phys. 86 (2004) 243–246.
[11] B. Jongsomjit, S. Ngamposri, P. Praserthdam, Catal. Letters 100 (2005) 139–146.
[12] B. Jongsomjit, E. Chaichana, P. Praserthdam, J. Mater. Sci. 40 (2005) 2043–2045.
[13] R. Mueller, R. Jossen, S.E. Pratsinis, M. Watson, M.K. Akhtar, J. Am. Ceram. Soc. 87 (2004) 197–202.
[14] J.C. Randall, J. Macromol. Sci., Rev. Macromol. Chem. Phys. C29 (1989) 201–315.
[15] G.B. Galland, P. Quijada, R.S. Mauler, S.C. deMenzes, Macromol. Rapid Commun. 17 (1996) 607–613.

Available online at www.sciencedirect.com
ScienceDirect
Materials Chemistry and Physics 100 (2006) 445–450
MATERIALS CHEMISTRY AND PHYSICS
www.elsevier.com/locate/matchemphys

Preparation and phase transformation behavior of χ-alumina via solvothermal synthesis

Okorn Mekasuwandumrong [a,*], Varong Pavarajarn [b], Masashi Inoue [c], Piyasan Praserthdam [b,*]

[a] *Department of Chemical Engineering, Faculty of Engineering and Industrial Technology, Silpakorn University, Nakorn Pathom 73000, Thailand*
[b] *Research Center on Catalysis and Catalytic Reaction Engineering, Department of Chemical Engineering, Faculty of Engineering, Chulalongkorn University, Bangkok 10330, Thailand*
[c] *Department of Energy and Hydrocarbon Chemistry, Graduate School of Engineering, Kyoto University, Kyoto 606-8077, Japan*

Received 9 August 2005; received in revised form 21 November 2005; accepted 23 January 2006

Abstract

Solvothermal reaction of aluminum isopropoxide (AIP) in mineral oil at 250–300 °C over 2 h duration provides χ-alumina powder, which transforms directly to α-alumina after calcination at high temperature. The mechanism of the crystallization process appears to be the initial formation of a spherical complex which subsequently decomposes further to precipitate a solid. This mechanism is suggested by XRD, IR, TG/DTA, SEM and TEM characterization of the powder formed. χ-Alumina attains a critical crystallite size around 15 nm through accretion on calcination and then transforms directly to α-alumina through nucleation and growth process. Direct α-phase transformation of χ-alumina powders rather than passage through κ-alumina can be explained by the absence of the cation contamination and the higher crystallinity of χ-alumina in the AIP decomposition process.

Keywords: Solvothermal; Direct transformation; χ-Alumina

1. Introduction

Alumina is one of the most common crystalline materials used in many applications such as adsorbents, coatings, soft abrasives, catalyst and catalyst support [1–3] due to its fine particle size, high surface area and catalytic activity. The structural stability of alumina also makes it an important constituent of many protective oxides formed on the surface of high temperature metals and alloys.

There are many metastable polymorphs of transition alumina, including χ-alumina. χ-Alumina is normally prepared by the dehydration of gibbsite (<200 nm) [3–5]. It transforms to κ-alumina at temperature around 650–750 °C before final transformation to α-alumina at 1000–1100 °C. Both transformations lead to loss in the surface area and changes in surface properties. Three different unit cells have been proposed for χ-alumina. Stumpf et al. [6] suggested that χ-alumina has a cubic unit cell with lattice parameter of 7.95 Å, whereas other researchers [4] proposed hexagonal unit cells with either $a = 5.56$ Å and $c = 13.44$ Å or $a = 5.57$ Å and $c = 8.64$ Å. Hexagonal χ-alumina possess a layered structure, in which the hexagonal arrangement of oxygen is inherited from the structure of gibbsite and aluminum occupies octahedral sites within the hexagonal structure.

Recently, Inoue et al. [7–10] have examined the thermal decomposition of metal alkoxides in inert organic solvents, e.g. glycols, and demonstrated that various kinds of novel crystalline product, including χ-alumina, can be directly obtained without bothersome procedures such as purification of the reactants or handling in inert atmosphere.

Nanocrystalline χ-alumina prepared from the thermal decomposition of AIP in inert organic solvent has high thermal stability. It transforms directly to α-alumina at the temperature around 1150 °C, without passing into the κ-phase [7,11,12], resulting in neither the loss in surface area nor the change in surface properties. Moreover, the abrupt crystal growth

* Corresponding authors. Tel.: +66 63116537; fax: +66 34219368.
E-mail address: okornm@yahoo.com (O. Mekasuwandumrong).

0254-0584/$ – see front matter © 2006 Elsevier B.V. All rights reserved.
doi:10.1016/j.matchemphys.2006.01.040

Table 1
The physical properties of as-synthesized products obtained by the thermal decomposition of AIP in mineral oil in various reaction conditions

Reaction conditions		Phase	Crystallite size (nm)	S_{BET} ($m^2\ g^{-1}$)	S_t ($m^2\ g^{-1}$)[a]	Pore volume ($cm^3\ g^{-1}$)[b]	Mode pore diameter (nm)[c]
Temperature (°C)	Time (h)						
250	0	Amorphous	–	7	7	0.03	11.8
250	2	χ-Alumina	9	192	186	0.64	13.3
250	6	χ-Alumina	10.8	149	189	0.43	11.5
270	2	χ-Alumina	10.2	180	210	0.52	11.5
300	2	χ-Alumina	9.4	124	138	0.45	14.2

[a] Calculated from the initial slope of the *t*-plot.
[b] Total nitrogen uptake at relative pressure of 0.98.
[c] Calculated from the desorption branch of the isotherm using the BJH method.

occurring during phase transformation can be effectively controlled. Therefore, nanocrystalline α-alumina can be simply obtained via the direct transformation from nanocrystalline χ-alumina. In this paper, we provide results for the reaction of AIP in mineral oil, including morphology of the synthesized particles and the phase transformation behavior.

2. Experiment

2.1. Sample preparation

Twenty-five grams of aluminum isopropoxide (AIP; Aldrich; >97%) was suspended in 100 ml of mineral oil (liquid paraffin; Ajax; specific gravity 0.830–0.890; CAS No. 8012-95-1) in a test tube, which was then set in a 300 ml autoclave. In the gap between the test tube and the autoclave wall, 30 ml of mineral oil was added. The autoclave was purged completely by nitrogen and heated up to the desired temperature, in the range of 250–300 °C, at a rate of 2.5 °C min^{-1}, and held at that temperature for the desired period of time (0–2 h). After the mixture was cooled down, the resulting powders were repeatedly washed with acetone and dried in air.

Parts of the product obtained was calcined in a box furnace by heating-up to the desired temperature (1000–1200 °C) at a rate of 10 °C min^{-1}. The calcination process was held at that temperature for 1 h.

2.2. Characterization

Powder X-ray diffraction (XRD) was measured on a SIEMENS XRD D5000 using Cu Kα radiation. The crystallite size was calculated from the Scherrer equation. The value of the shape factor, *K*, was taken to be 0.9 and α-alumina was used as an external standard. Infrared (IR) Spectra were recorded on a NICOLET FT-IR Impact 400 spectroscopy using an ex situ IR technique. The thermal behavior of the samples were analyzed on a Perkin-Elmer Diamond TG/DTA thermal analyzer at a heating rate of 10 °C min^{-1} in a 40 ml min^{-1} flow of dried air. Nitrogen adsorption isotherm and BET surface area of the samples were measured by a micromeritics medel ASAP 2000 using nitrogen as the adsorbate. The primary particles of alumina samples were observed by a JEOL TEM-200cx transmission electron microscope operated at 100 kV. Morphologies of alumina products were observed on JEOL scanning electron microscope.

3. Results and discussions

Table 1 summarizes the physical properties of obtained products before calcination. The products synthesized from the decomposition of AIP in mineral oil at 250, 270 and 300 °C with a holding time exceeding 2 h are χ-alumina, while the product obtained from heating the system up to 250 °C without holding time is amorphous. The amorphous product has much lower BET surface area and pore volume than all crystalline products. χ-Alumina obtained by the reaction at 250 °C for 2 h has the highest BET surface area and pore volume. When the reaction temperature is increased or the holding time is prolonged, BET surface area and pore volume of the obtained product is decreased by the coagulation of primary particles due to thermal effect.

The IR spectra of the products are shown in Fig. 1. All as-obtained powders show two adsorption bands attributed to water of crystallization at 3500–3200 cm^{-1} (υ(OH)) and 1640 cm^{-1} (δ(OH)) [13]. The amorphous powder obtained by quenching from 250 °C shows a strong adsorption bands at 1340–1470 cm^{-1} due to the isopropyl hydrocarbon groups [13]. As the holding time or reaction temperature is increased, the adsorption bands due to the organic group decrease and eventually disappear. The characteristic bands of boehmite were detected at 773 and 615 cm^{-1} [10] in the products obtained from 2 h reaction at 250 and 300 °C. This observation can be explained by the formation of boehmite by hydrolysis of AIP with water produced during the reaction.

Fig. 2 shows the results from the thermogravimetric analysis, i.e. TGA and DTA plots, of all powders prepared in mineral oil using various reaction conditions. Two weight decrease processes were detected from the amorphous powder corresponding on one endothermic and exothermic process. The first decrease in mass at around 80–200 °C, accompanied by the endothermic peak in DTA signal, is attributed to the desorption of physisorbed water. The second sharp mass decrease in TGA plot with sharp exothermic peak in DTA plot at around 300 °C is attributed to the combustion of organic moiety. The overall mass loss of this

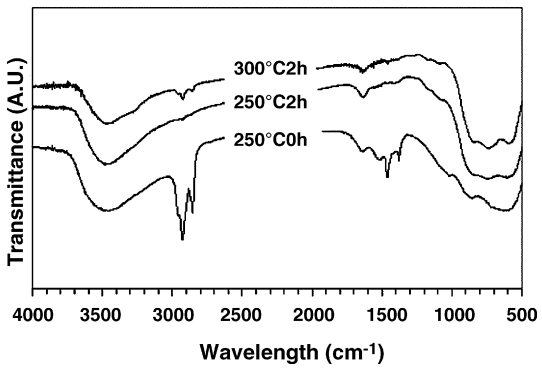

Fig. 1. IR spectra of as-synthesized products at various reaction conditions.

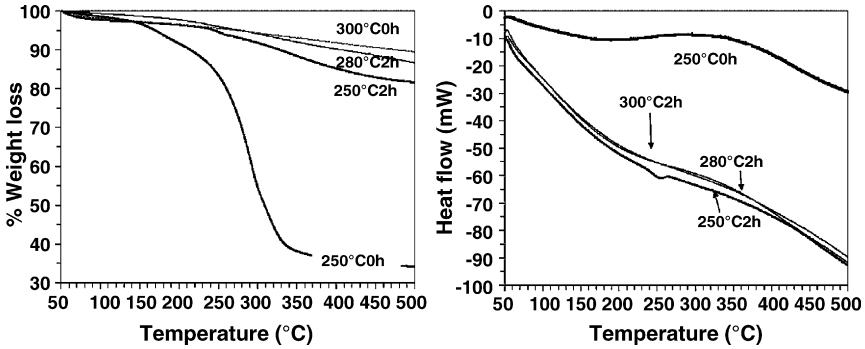

Fig. 2. TG and DTA data of the as-synthesized products.

amorphous sample is around 45%, which is lower than theoretically loss for AIP decomposition (75%). It is indicated that the starting AIP partially decomposes in mineral oil during the heating-up process. The remaining organic moieties from the partial decomposition of AIP reside in the amorphous product.

The nitrogen adsorption isotherms of as-synthesized products are shown in Fig. 3. All the crystalline samples exhibit the hysteresis loop with type-A adsorption characteristic, which is corresponding to the presence of two-ended tabular pore structure. On the other hand, the amorphous product shows the type-E hysteresis loop, which is an indication for the presence of tabular, through short pores with winded parts of various widths [14,15]. These pores are formed among the primary particles of alumina. Fig. 4 presents the pore size distribution of as-synthesized. All crystalline products exhibited the typical characteristic of mesopore system with pore size around 10 nm. It is shown that all products have narrow size distribution.

Fig. 5 shows the morphologies of as-synthesized and calcined samples observed by SEM. Spherical particles with average diameter around 1.8 μm were observed in the amorphous products prepared by quenching the reaction after the temperature had reached 250 °C (Fig. 5a). For the reaction with the holding

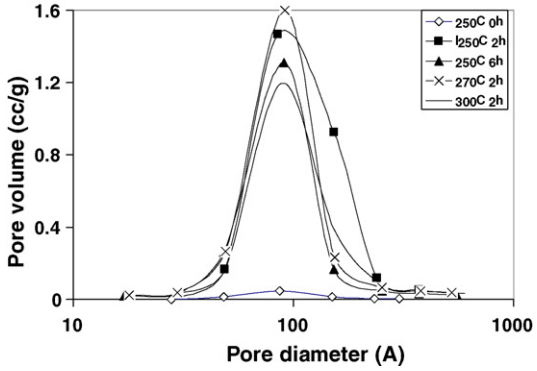

Fig. 4. Pore size distribution of as-synthesized product.

time prolonged to 2 h, similar spherical particles in the products can still be observed. However, the average size of the particles decreases to 1.2 μm (Fig. 5b). These particles are secondary aggregates of nanocrystalline χ-alumina. With the increase of reaction temperature to 300 °C, size of the secondary particles further decreases to 1 μm (Fig. 5c). The results suggest that AIP decomposes stepwise in the inert solvent during heating-up

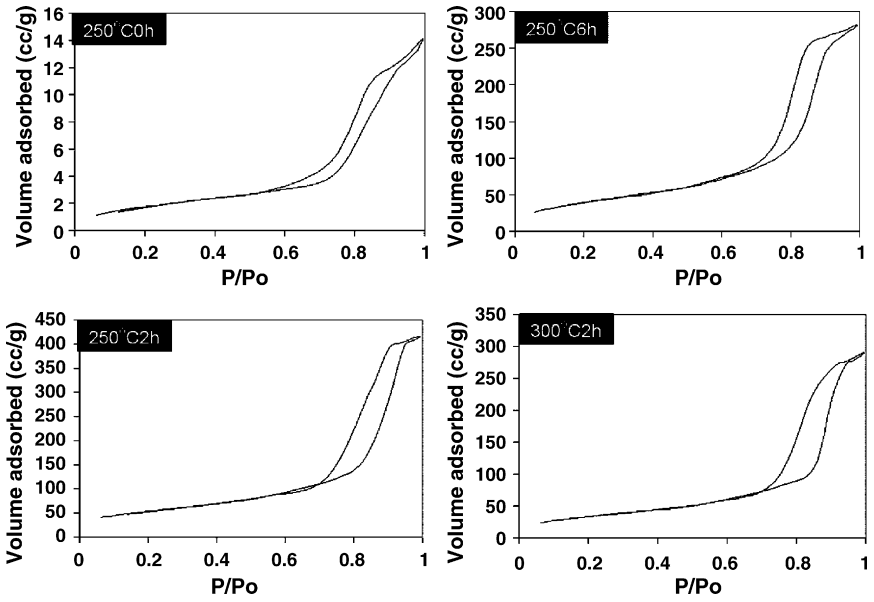

Fig. 3. The nitrogen adsorption isotherms of as-synthesized products.

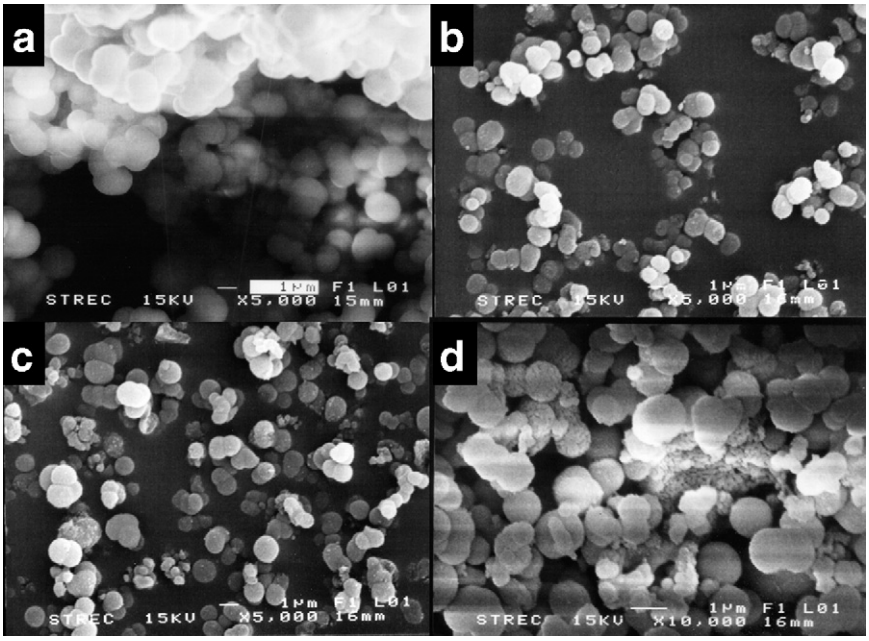

Fig. 5. SEM images: (a) as-synthesized product prepared by quenching reaction in mineral oil at 250 °C, (b) as-synthesized product prepared in mineral oil at 250 °C for 2 h, (c) as-synthesized product prepared in mineral oil at 300 °C for 2 h and (d) product (b) calcined at 1150 °C.

process, which results in an intermediate complex suspending in mineral oil. SEM micrographs confirms that this complex assumes a spherical shape. During the holding period, the complex further decomposes giving the nanocrystalline χ-alumina aggregated in form of spherical particles. The decrease in particle size with the increase in holding time and reaction temperature is due to the loss of the organic moiety in the complex by further decomposition. In this case, there are two nucleation processes. The first nucleation process is the formation of tiny droplets of the intermediate complex. This process is related to the salting out phenomena. During the partial decomposition of organic moieties, the decomposed intermediate is supersaturated in the solution and it is salted out forming the glassy droplets. Because the number of droplets formed in mineral oil is small, the droplets grow and large spherical particles are obtained. The second nucleation step is the formation tiny crystallites of χ-alumina. The morphology of products obtained in this work is different from χ-alumina obtained from the reaction in toluene [12]. This result will be further discussed.

According to Derjaguin–Landua–Verwey–Overbeek (DLVO) theory, the energy barrier between two particles, which inhibit agglomeration, is expressed as follow:

$$V_b = \left(\frac{A\kappa\alpha}{12}\right) + 2\pi\varepsilon_0\varepsilon_r\kappa\alpha\phi^2$$

where A is the effective Hamaker constant, κ the Debye–Huckel parameter, α the particle diameter, ε_0 the permittivity in the free space, ε_r the dielectric constant of the continuous phase and ϕ is the particle surface potential. Because of the constant ionic strength of the solvent, ε_0 and κ is constant, the maximum repulsive force estimated from the second term of the right hand side of the equation ($2\pi\varepsilon_0\varepsilon_r\kappa\alpha\phi^2$) is determined by the dielectric constant, particle size and repulsive force. Mineral oil (liquid paraffin) is the mixtures of long straight chain hydrocarbon produced as the bottom product from distillation. The dielectric constant of long chain hydrocarbon is around 1.9–2 ($C_{13}H_{28} = 2.02$, $C_{14}H_{30} = 2.05$, $C_{19}H_{40} = 2.09$), which lower than toluene (2.379). According to the quite low dielectric constant of mineral oil, the particles become discrete and form spherical particles. Fang and Chen [16] reported that, for the synthesis of TiO_2 by the reaction of $TiCl_4$ in a mixed solvent of *n*-propanol and water, the spherical particles were

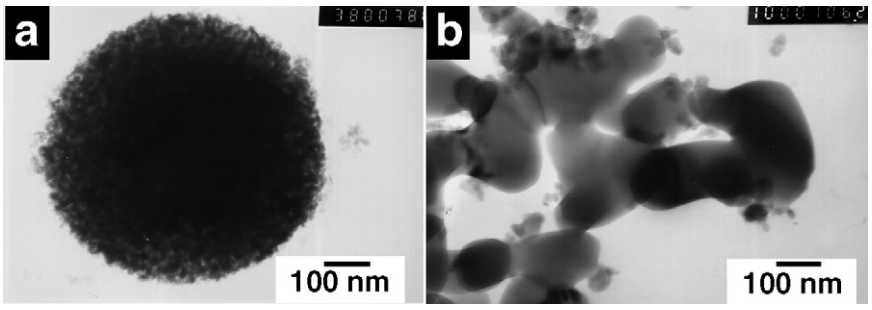

Fig. 6. TEM images: (a) as-synthesized product prepared in mineral oil at 250 °C for 2 h and (b) product (a) calcined at 1150 °C.

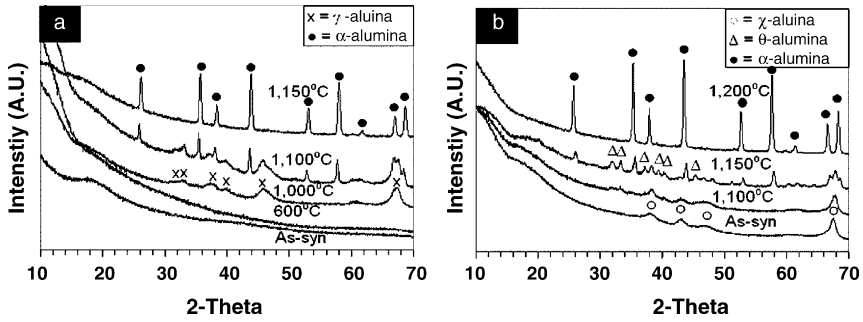

Fig. 7. The XRD patterns of powder synthesized by the reaction of AIP in mineral oil calcined at various reaction conditions: (a) 250 °C for 0 h and (b) 300 °C for 2 h.

formed in the solvent with *n*-propanol/water ratio resulting in the lowest value of dielectric constant.

Transmission electron micrographs of the as-obtained powder and calcined powder are shown in Fig. 6. The as-synthesized χ-alumina products are comprised of agglomerated primary particles having average diameter around 10 nm. As shown in Table 1, the crystallite size calculated by XRD peak broadening, using the Scherrer equation, is 9 nm. Good agreement between both values indicates that each primary particle observed by TEM is a single crystal of χ-alumina.

The XRD patterns of calcined product are shown in Fig. 7. The amorphous product remains amorphous even after calcination at 600 °C (Fig. 7a). However, after calcination at 1000 °C, γ-alumina is observed. The α-phase transformation takes place at temperature around 1150 °C and completes at 1200 °C. It should be noted that the peak at 42.5°, which is corresponding to χ-alumina, is not detected. This indicates that χ-alumina is not formed by calcination of the amorphous product. Therefore, the formation of χ-alumina occurs only in the inert organic solvent. For the calcination of χ-alumina obtained from thermal decomposition of AIP at 300 °C for 2 h (Fig. 7b), χ-alumina transforms to α-alumina directly at temperature around 1100 °C. No κ-alumina was detected. The χ-to-α phase transformation is completed at temperature around 1200 °C. Phase transformation sequences of products obtained from other reaction conditions are summarized in Table 2.

After calcination, the secondary particles still remain spherical with unchanged average particle size, regardless of the crystalline phase (see Fig. 5d). Some finger-like primary particles aggregating on the spherical secondary particles were also observed after the calcination at 1200 °C. TEM micrographs of calcined samples clearly show two groups of primary particles after the phase transformation. The first group is the spherical χ-alumina particles, which do not transform to α-alumina. These particles have crystallite size calculated from the Scherrer equation that is the same as particle size observed by using TEM. The second group of primary particles is the finger-like α-alumina transformed from the low-temperature transition alumina nanocrystals via the nucleation and growth mechanism (see Fig. 6b).

The direct phase transformation of χ- to α-alumina is a specific property for powders prepared by the decomposition of AIP in an inert organic solvent. In our previous work, it has been proposed that the direct phase transformation is the result from the absence of contaminating cations in crystals, as well as high crystallinity of the synthesized product due to the small amount of water adsorbed on the surface. Chou and Nieh [17] have reported that the nucleation of α-alumina occurs along (2 2 0) crystallographic plane of γ-alumina in nanocrystalline oxide synthesized by radio frequency reactive sputtering deposition. Johnston et al. [18] have reported that γ-alumina prepared by laser ablation synthesis directly transforms into α-phase and they have attributed that the particle size of the product is well below the grain size limit for super plastic alumina (500 nm). Bahlawane and Watanabe [19] prepared anhydrous alumina which transformed directly to α-alumina by sol–gel method. Shek et al. [20] have reported that amorphous powders prepared by oxidation of pure aluminum metal crystallize to γ-alumina, which directly transforms to α-alumina at 1370 K. They have attributed this result to the facilitation of nucleation of α-alumina by the strain relaxation of the transition alumina lattice. However, relaxation of the γ-alumina structure should decrease the energy level of γ-alumina and disturb the nucleation of more stable phases. Simpson et al. [21] have reported that samples prepared via electron-beam evaporation of alumina onto a sapphire substrate held at room temperature crystallize to γ-alumina, which transforms into α-alumina without formation

Table 2
The crystallite size calculated by the Scherrer equation and phase of the as-synthesized and calcined products

Reaction condition		Crystallite size and phase of alumina after treat at various temperatures (°C)				
Temperature (°C)	Time (h)	As-synthesized	1000	1100	1150	1200
250	0	– (Amorphous)	6.2 (γ)	16.5 (γ), 31.1 (α)	33.7 (α)	– (α)
250	2	9 (χ)	9.2 (χ)	9.6 (χ)	12.3 (χ), 36.4 (α)	68 (α)
250	6	10.8 (χ)	11.2 (χ)	12.5 (χ)	15.2 (χ), 39.2 (α)	77.2 (α)
270	2	10.2 (χ)	9.4 (χ)	10.3 (χ)	15.6 (χ), 33.5 (α)	97.5 (α)
300	2	9.4 (χ)	10.8 (χ)	14.2 (χ), 39.5 (α)	14.6 (χ), 41.3 (α)	44.7 (α)

of other intermediate phases. They have attributed this result to the epitaxial growth of α-alumina on the sapphire substrate. Ogihara et al. [22] have prepared monodispersed, spherical alumina by the controlled hydrolysis of aluminum alkoxide in a dilute solution containing octanol and acetonitrile. They have found that the amorphous product crystallizes to γ-alumina at 1000 °C which converted to α-alumina at 1150 °C without intermediate phase. However, they did not give any explanation for this result. It has also reported that γ-alumina formed by thermal decomposition of aluminum sulfate transforms into α-alumina directly [23–25].

The crystallite sizes of calcined products are summarized in Table 2. The crystallite size of is initially about 9–10 nm. χ-Alumina grows to 16 nm upon calcination but the growth stop at this size even after the calcination at high temperature. At higher calcination temperature, only α-alumina was observed. It is suggested that χ-alumina grows to the critical size and then abruptly transforms into α-alumina. The result suggests that the critical size of χ-alumina, beyond which it is unstable and undergoes phase transformation into α-alumina, is around 16 nm. Once the phase transformation takes place, the primary particles grow drastically and then become sluggish. The α-phase transformation is considered to occur through a nucleation and growth mechanism [26,27]. Investigations on the phase transformation after the crystallite size has reach the critical size have been reported by many researchers [28–30]. Yen et al. [28,29] have found that, during the phase transformation, there is a critical size for θ-alumina (around 22 nm) at the nucleation stage, which initiates the formation of α-alumina nucleus.

4. Conclusion

Thermal decomposition of AIP in mineral oil at temperature between 250 and 300 °C with holding time of 2 h results in the micro-spherical particles formed by agglomeration of nanocrystalline χ-alumina. On the contrary, the powder obtained during the heating-up process to 250 °C is amorphous. The fact that χ-alumina is not formed by the calcination of the amorphous intermediate confirms that χ-alumina is formed only by AIP decomposition in the inert organic solvent. It is suggested that a spherical particle of complex moieties forms through stepwise decomposition of AIP in the solvent. With the prolonged holding time or increased reaction temperature, this complex sheds organic moieties and solid-state phase of χ-alumina is formed. After calcination at high temperature, χ-alumina transformed to α-alumina directly. The crystallite size of χ-alumina is initially around 9–10 nm and grows upon the calcination to the critical size of 16 nm, beyond which χ-alumina transforms to α-alumina. This direct transformation behavior of nanocrystalline χ-alumina is attributed to the absence of cations and the less defect structure.

Acknowledgement

The author would like to thank the Thailand Research Fund (TRF) for their financial support.

References

[1] W.H. Gitzen, Alumina as a Ceramics Material, American Ceramic Society, Columbus, OH, 1970.
[2] G.M. Pajonk, Appl. Catal. A: Gen. 72 (2) (1991) 217–266.
[3] K. Wefers, G.M. Bell, Oxides and Hydroxides of Alumina, Alcoa, Bauxite, AR, 1972.
[4] H. Saalfeld, Structure Phases of Dehydrated Gibbsite, Elsevier, The Netherlands, 1961.
[5] G.W. Brindley, J.O.T. Choe, Am. Miner. 46 (7–8) (1961) 771785.
[6] H.C. Stumpf, A.S. Russell, J.W. Newsome, C.M. Tucker, Ind. Eng. Chem. 42 (7) (1950) 1398–1403.
[7] M. Inoue, H. Kominami, T. Inui, J. Am. Ceram. Soc. 75 (9) (1992) 2597–2598.
[8] M. Inoue, H. Kominami, T. Inui, Appl. Catal. A: Gen. 121 (1) (1995) L1–L5.
[9] S. Iwamoto, K. Saito, M. Inoue, K. Kagawa, Nano Lett. 1 (8) (2001) 417–421.
[10] P. Pratherthdam, M. Inoue, O. Medkasuvandumrong, W. Thanakulrangsan, S. Phatanasri, Inorg. Chem. Commun. 3 (11) (2000) 671–676.
[11] O. Mekasuwandumrong, P.L. Silveston, P. Praserthdam, M. Inoue, V. Pavarajarn, W. Tanakulrungsank, Inorg. Chem. Commun. 6 (7) (2003) 930–934.
[12] O. Mekasuwandumrong, H. Kominami, M. Inoue, P. Praserthdam, J. Am. Ceram. Soc. 87 (8) (2004) 1543–1549.
[13] D.A. Skoog, J.J. Leary, Principles of Instrumental Analysis, Saundres College Publishing, Philadelphia, San Diego, 1992.
[14] B.C. Lippens, J.H. de Boer, J. Catal. 4 (3) (1965) 319–323.
[15] B.C. Lippens, J.H. de Boer, J. Catal. 3 (1) (1964) 32–37.
[16] C. Fang, Y. Chen, Mater. Chem. Phys. 78 (3) (2003) 739–745.
[17] T.C. Chou, T.G. Nieh, J. Am. Ceram. Soc. 74 (9) (1991) 2270–2279.
[18] G.P. Johnston, R. Muenchausen, D.M. Smith, W. Fahrenholtz, S. Foltyn, J. Am. Ceram. Soc. 75 (12) (1992) 3293–3298.
[19] N. Bahlawane, T. Watanabe, J. Am. Ceram. Soc. 83 (9) (2000) 2324–2326.
[20] C.H. Shek, J.K.L. Lai, T.S. Gu, G.M. Lin, Nanostruct. Mater. 8 (5) (1997) 605–610.
[21] T.W. Simpson, Q. Wen, N. Yu, D.R. Clarke, J. Am. Ceram. Soc. 81 (1) (1998) 61–66.
[22] T. Ogihara, H. Nakagawa, T. Yanagawa, N. Ogata, K. Yoshida, J. Am. Ceram. Soc. 74 (9) (1991) 2263–2269.
[23] D.W. Johnson, F.J. Schnettler, J. Am. Ceram. Soc. 53 (8) (1970) 440–444.
[24] E. Kato, K. Daimon, M. Nanbu, J. Am. Ceram. Soc. 64 (8) (1981) 436–445.
[25] M.D. Sacks, T.-Y. Tseng, S.Y. Lee, Ceram. Bull. 63 (2) (1984) 301–310.
[26] D.S. Tucker, J. Am. Ceram. Soc. 68 (7) (1985) C163–C164.
[27] F.W. Dynys, J.W. Halloran, J. Am. Ceram. Soc. 65 (9) (1982) 442–448.
[28] F.S. Yen, H.L. Wen, Y.T. Hsu, J. Crystal Growth 233 (4) (2001) 761–773.
[29] F.S. Yen, H.S. Lo, H.L. Wen, R.J. Yang, in press.
[30] R.B. Bagwell, G.L. Messing, P.R. Howell, J. Mater. Sci. 36 (7) (2001) 1833–1841.

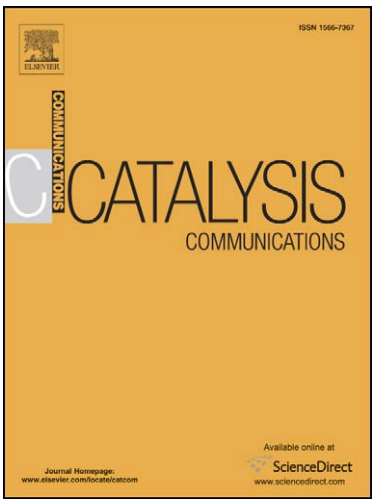

Effect of Mixed γ and χ Crystalline Phases in Nanocrystalline Al_2O_3 on the Dispersion of Cobalt on Al_2O_3

Kamonchanok Pansanga, Joongjai Panpranot, Okorn Mekasuwandumrong, Chairit Satayaprasert, James G. Goodwin, Jr., Piyasan Praserthdam

PII: S1566-7367(07)00244-0
DOI: 10.1016/j.catcom.2007.05.042
Reference: CATCOM 1276

To appear in: *Catalysis Communications*

Received Date: 10 January 2007
Revised Date: 22 May 2007
Accepted Date: 22 May 2007

Please cite this article as: K. Pansanga, J. Panpranot, O. Mekasuwandumrong, C. Satayaprasert, J.G. Goodwin, Jr., P. Praserthdam, Effect of Mixed γ and χ Crystalline Phases in Nanocrystalline Al_2O_3 on the Dispersion of Cobalt on Al_2O_3, *Catalysis Communications* (2007), doi: 10.1016/j.catcom.2007.05.042

"REVISED II"

Effect of Mixed γand χ Crystalline Phases in Nanocrystalline Al_2O_3 on the Dispersion of Cobalt on Al_2O_3

Kamonchanok Pansanga[a], Joongjai Panpranot[a], Okorn Mekasuwandumrong[b], Chairit Satayaprasert[a], James G. Goodwin, Jr.[c], and Piyasan Praserthdam[*,a]

[a] Center of Excellence on Catalysis and Catalytic Reaction Engineering, Department of Chemical Engineering, Faculty of Engineering, Chulalongkorn University, Bangkok 10330, Thailand

[b] Department of Chemical Engineering, Faculty of Engineering and Industrial Technology, Silpakorn University, Nakorn Pathom 73000, Thailand

[c] Department of Chemical and Biomolecular Engineering, Clemson University, Clemson, South Carolina, 29634, USA

Keywords: nanocrystalline alumina; crystalline phase; cobalt catalyst; CO hydrogenation; χ alumina; γalumina

Submitted to: *Catalysis Communications*

Date: May 22, 2007

[*] All correspondence should be addressed.